Nanoconfined NaAlH 4 : Determination of Distinct Prolific Effects from Pore Size, Crystallite Size, and Surface Interactions

ARTICLE *in* THE JOURNAL OF PHYSICAL CHEMISTRY C · OCTOBER 2012

Impact Factor: 4.77 · DOI: 10.1021/jp3049982

6 AUTHORS, INCLUDING:

Payam Javadian
Aarhus University
13 PUBLICATIONS **125** CITATIONS
SEE PROFILE

Marek Polanski
Military University of Technology
43 PUBLICATIONS **427** CITATIONS
SEE PROFILE

Flemming Besenbacher
Aarhus University
642 PUBLICATIONS **25,636** CITATIONS
SEE PROFILE

Torben Rene Jensen
Aarhus University
247 PUBLICATIONS **4,645** CITATIONS
SEE PROFILE

THE JOURNAL OF PHYSICAL CHEMISTRY C

Article

pubs.acs.org/JPCC

Nanoconfined $NaAlH_4$: Determination of Distinct Prolific Effects from Pore Size, Crystallite Size, and Surface Interactions

Thomas K. Nielsen,[†] Payam Javadian,[†] Marek Polanski,[‡] Flemming Besenbacher,[§] Jerzy Bystrzycki,[‡] and Torben R. Jensen*,[†]

[†]Center for Energy Materials, Interdisciplinary Nanoscience Center (iNANO), and Department of Chemistry, Aarhus University, DK-8000 Aarhus, Denmark

[‡]Faculty of Advanced Technology and Chemistry, Military University of Technology, 2 Kaliskiego Strasse, 00-908 Warsaw, Poland

[§]Interdisciplinary Nanoscience Center (iNANO) and Department of Physics and Astronomy, Aarhus University, DK-8000 Aarhus C, Denmark

Supporting Information

ABSTRACT: Nanoconfinement is a new method to improve the hydrogen storage properties for metal hydrides. A systematic study of melt-infiltrated $NaAlH_4$ in resorcinol formaldehyde carbon aerogels with pore sizes of D_{max} = 4, 7, 10, 13, 19, 22, 26, 39 and >100 nm is presented. A linear correlation between pore size and crystalline domain size is observed using PXD. The distinct effects from pore size, crystallite size, and interfacial contact between $NaAlH_4$ and carbon aerogel on hydrogen release and uptake properties are investigated. In situ synchrotron powder X-ray diffraction shows that formation of crystalline $NaAlH_4$ nanoparticles only occurs in the nanoporous scaffolds ($4 < D_{max} < 100$ nm). The hydrogen desorption kinetics are significantly improved by confinement in the macroporous scaffold ($D_{max} > 100$ nm) as compared to bulk $NaAlH_4$, i.e., reduction of the temperature for maximum hydrogen release rate of $\Delta T_{max} = -90$ °C. Additional improvement is induced by reducing the pore sizes in the range $7 \leq D_{max} \leq 39$ nm and thereby the $NaAlH_4$ crystallite sizes, but this effect is small ($\Delta T_{max} = -12$ to -16 °C) relative to the catalytic effects induced by the aerogel surface. Sieverts' measurements reveal similar stability and preserved reversible hydrogen storage capacity after four hydrogen release and uptake cycles for both nano- (D_{max} = 13 nm) and macroporous scaffolds (D_{max} > 100 nm) of ~53% of the original capacity. The results suggests that a significant contribution to the observed improvements of kinetics and reversibility by nanoconfinement of $NaAlH_4$ in carbon aerogels can be assigned to the catalytic properties of the scaffold surfaces and a minor contribution arises from nanoconfinement and reduction of the pore size in the range of 39−7 nm.

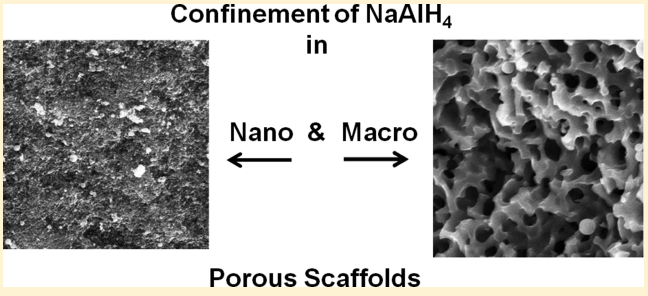

1. INTRODUCTION

Hydrogen is recognized as a clean and sustainable energy carrier with gravimetric energy density three times larger than that of gasoline.[1] Unfortunately, hydrogen is a gas at ambient conditions and is therefore difficult to store in an efficient and compact way. On one hand, the hydrogen molecule, H_2, with only two electrons forms the weakest van der Waals (dispersion) interaction of all molecules. On the other hand, hydrogen forms relatively strong bonds to most elements, which calls for the use of a catalyst or other means of facilitating hydrogen release and uptake, e.g., nanoconfinement.

Confinement of metal hydrides in a nanoporous material is a *bottom-up* approach, which creates nanoparticles. This limits the particle size of the hydride to the pore size of the scaffold material, which allows direct production of smaller particles than mechanically obtainable. Furthermore, particle growth and agglomeration may be hindered by the compartmentalization of nanoparticles within the scaffold material and also limit the mobility of the decomposition products and keep them in intimate close contact. Thereby, *nanoconfinement* may improve both hydrogen release and uptake properties of metal hydrides.[2−5]

The ideal solid-state hydrogen-containing material should facilitate compact, safe, and inexpensive storage. Furthermore, hydrogen release and uptake must be fast at low temperatures (-40 °C < $T_{release/uptake}$ < 80 °C) controlled by the hydrogen pressure.[1,6,7] Sodium aluminum hydride, $NaAlH_4$, is a promising candidate owing to appropriate thermodynamic properties and reasonable hydrogen densities of ρ_m = 7.5 wt % H_2 and ρ_V = 94 g H_2/L.[8] Hydrogen is released in three steps according to the reaction scheme I:

$$3NaAlH_4(s) \rightleftarrows Na_3AlH_6(s) + 2Al(s) + 3H_2(g) \quad \text{(I)}$$

$$Na_3AlH_6(s) \rightleftarrows 3NaH(s) + Al(s) + (3/2)H_2(g) \quad \text{(II)}$$

Received: May 23, 2012
Revised: September 5, 2012
Published: September 5, 2012

$$NaH(s) \rightleftarrows Na(l) + (1/2)H_2(g) \quad \text{(III)}$$

Although favorable hydrogen release temperatures of 18 and 103 °C are predicted from the reaction enthalpies of ΔH_D = 33.1 and 49.0 kJ/mol H_2 at $p(H_2)$ = 1 bar for steps I and II, respectively,[8−10] the actual hydrogen release occurs at higher temperatures of T_I > 180, T_{II} > 240 °C, and T_{III} > 425 °C. Due to the high stability of NaH, the practical hydrogen content of $NaAlH_4$ is considered to be 5.6 wt % H_2. Furthermore, NaH and Al is not easily rehydrogenated to form $NaAlH_4$.

The kinetics for hydrogen release and uptake can be significantly improved by ball milling with Ti-based additives.[11−14] As an alternative, $NaAlH_4$ has recently been melt-infiltrated into carbon-based nanoporous materials. Nanoconfinement of $NaAlH_4$ improves hydrogen release and uptake kinetics and the reversible hydrogen storage capacity.[2,9,15−18] These favorable properties may be linked to the formation of reactive nanoparticles. However, ball milling $NaAlH_4$ with additives such as carbon aerogels, carbon nanotubes, and fullerenes also catalyzes the dehydrogenation as well as the hydrogenation of $NaAlH_4$.[19,20] The most efficient to date is nanoconfinement of $NaAlH_4$ in Ti-functionalized carbon aerogel scaffolds (D_{max} = 17 nm). Hydrogen release has an onset temperature of 33 and maximum release rate at 125 °C with a heating rate of 5 K/min.[16]

In this work, $NaAlH_4$ is nanoconfined in resorcinol formaldehyde carbon aerogels with pore sizes ranging from large macropores (>100 nm) to small nanopores (<4 nm). The impacts on the hydrogen desorption kinetics and reversible hydrogen storage capacity are investigated. The aim of this study is to distinguish among effects originating from the nanopores, nanoparticle sizes, and the catalytic properties of the scaffold surface.

2. EXPERIMENTAL DETAILS

2.1. Sample Preparation. The resorcinol formaldehyde aerogels, denoted X, were prepared by mixing selected amounts of resorcinol (Aldrich, 99%), formaldehyde in water (37 wt % stabilized by ∼10−15% methanol, Merck), deionized water, and Na_2CO_3 (Aldrich, 99.999%) in a beaker with continuous stirring. The pH value of the final solution was recorded; see Table 1. Afterward the preparation and characterization were performed according to previously published procedures.[21,22]

Prior to use, all aerogels were activated at 400 °C in vacuum for several hours in order to remove moisture and gases from the porous structure. All subsequent handling was performed in a purified argon atmosphere in a glovebox. Samples of aerogels loaded with $NaAlH_4$ were prepared by grinding monoliths of aerogel together with $NaAlH_4$ (Aldrich, 90%), obtaining a powder. The amount of $NaAlH_4$ was adjusted to obtain the same degree of pore filling of approximately 60 vol % for all samples; i.e., the quantity was calculated on the basis of the total pore volume, V_{tot}, of the aerogel and the bulk density of $NaAlH_4$ (ρ = 0.905 g/mL) (see Table 2).[9,15,16,23] Melt infiltration was performed under inert conditions in a custom-made manually operated hydrogenation station by heating to a temperature of 189 °C, reaching hydrogen pressures in the range of 210−230 bar ($\Delta T/\Delta t$ = 2.6 °C/min). The sample temperature was kept fixed at 189 °C for 15 min, and then the sample was cooled naturally. Selected nanoconfined samples were carefully mixed with Si (standard reference material NBS 640a with a mean crystallite size of 2 μm) and used for SR-PXD studies; see the Supporting Information.

Table 1. Reactants Used for Synthesis of Resorcinol Formaldehyde Aerogels, Denoted X

aerogel	resorcinol/g	formaldehyde/mL	H_2O/mL	Na_2CO_3/g	pH
X4	20.681	28.5	28.3	0.060	6.70
X7	20.710	28.5	28.3	0.039	6.44
X10	41.618	56.9	56.6	0.065	6.24
X13	41.333	56.9	56.6	0.051	6.18
X19[a]	41.333	56.9	56.6	0.049	6.15
X22[a]	41.429	56.9	56.6	0.035	6.06
X26	41.429	56.9	56.6	0.034	6.03
X39	41.771	56.9	56.6	0.018	5.77
X > 100	41.503	56.9	56.6	0	3.57

[a]During the preparation the aerogel was aged for 72 h at RT followed by 48 h at 90 °C. (Normal procedure is 24 h at RT, 24 h at 50 °C, and 72 h at 90 °C).[21]

2.2. Scanning Electron Microscopic (SEM). SEM images were acquired with a Nova NanoSEM 600 from FEI. The samples were mounted on carbon tape supported by an aluminum sample holder and transported to the apparatus with air exposure.

2.3. Synchrotron Radiation Powder X-ray Diffraction Measurements. Synchrotron radiation powder X-ray diffraction (SR-PXD) data were collected at beamline I711 at MAX-lab, Lund, Sweden.[24] A ca. 10 mm long powder sample was mounted in a sapphire capillary tube with an inner diameter of 0.79 mm and placed in an airtight sample holder under inert conditions in an argon-filled glovebox.[24] The sample holder was moved from the glovebox to the diffractometer without exposing the sample to air. The selected X-ray wavelength was λ = 0.989 Å, and data were collected using a CCD detector.

2.4. Sieverts' Measurements. The cyclic stability of selected samples was studied by Sieverts' measurements (PCTpro 2000) of four hydrogen release and uptake cycles. The samples were transferred to an autoclave, which was sealed under argon in a glovebox and attached to the apparatus. Hydrogen desorption data were collected in the temperature range from RT to 200 °C, at $p(H_2) = 10^{-2}$ bar, and with the temperature kept fixed at 100 °C for 4 h, at 150−152 °C for 4 h, and at 200−203 °C for 8 h ($\Delta T/\Delta t$ = 0.5 °C/min). Hydrogen absorption was performed at $p(H_2)$ = 89−92 bar and at a temperature of 160 °C for 10 h, and the sample was cooled to RT naturally ($\Delta T/\Delta t$ = 5 °C/min).

2.5. Temperature-Programmed Desorption Mass Spectroscopy. A Setaram Sensys Evo differential scanning calorimeter (horizontal position) coupled with a Hiden Analytical quadrupole mass spectrometer (MS) under a constant flow (28 mL/min) of ultrahigh-purity helium (<10 ppb O_2 and H_2O, Air Products) was used for temperature-programmed desorption mass spectroscopy (TPD-MS) measurements. A powdered sample (<20 mg) was placed in an Al_2O_3 crucible with lid and then encapsulated in a protective aluminum crucible. Loading of the samples was performed without air contact in a glovebox. The samples were purged with helium for at least 2 h and heated in the temperature range 20−450 °C ($\Delta T/\Delta t$ = 1 °C/min). During the experiment the MS signals at m/e = 2, 18, and 32 were recorded in order to detect H_2, H_2O, and O_2. No significant quantity of H_2O or O_2 was detected.

dx.doi.org/10.1021/jp3049982 | J. Phys. Chem. C 2012, 116, 21046−21051

Table 2. Morphological Parameters for the Pristine Carbon Aerogel Scaffold Materials[a]

sample	S_{BET} (m^2/g)	V_{meso} (mL/g)	V_{tot} (mL/g)	V_{micro}/V_{tot}	D_{max} (nm)	$NaAlH_4$ (wt %)	$NaAlH_4$ (vol %)
std. dev.[b]	±12	±0.02	±0.02	±0.01	±0.5	±0.02	±2
X4	584	0.11	0.36	0.40	<4	12.8	50
X7	677	0.51	0.69	0.24	7	27.3	60
X10	704	0.74	0.91	0.19	10	34.1	63
X13	639	0.67	0.86	0.20	13	31.8	60
X19	718	1.12	1.33	0.14	19	41.9	60
X22	625	1.23	1.39	0.13	22	43.0	60
X26	659	1.10	1.30	0.15	26	41.4	60
X39	634	0.88	1.09[c]	0.16	39[c]	37.2	–[c]
X > 100	588	0.02	0.26[c]	0.88	>100	32.0	–[c]

[a]Gravimetric and volumetric amounts of infiltrated $NaAlH_4$ are also provided. [b]Standard deviation is based on the homogeneity studies of aerogel X10. [c]Value is not estimated accurately due to the formation of macropores.

3. RESULTS AND DISCUSSION

3.1. Nanoporous Aerogel Materials. Nine porous resorcinol formaldehyde carbon aerogels were synthesized for this study, and their texture parameters are listed in Table 2.[22] The aerogels were prepared with systematic variation of the peak value for the pore size distributions, D_{max}, of 4, 7, 10, 13, 19, 22, 26, and 39 nm, which are denoted X4, X7, etc. The homogeneity of aerogel X10 was further investigated (see the Supporting Information) revealing standard deviations for the morphological parameters; see Table 2. An aerogel, denoted X > 100, has micropores but also large macropores for which the D_{max} value cannot be determined using nitrogen gas sorption. Large macropores ($D \gg 100$ nm) do not lead to nitrogen gas condensation during the gas sorption analysis and therefore do not contribute to the recorded pore volume, V_{tot}. This explains the observed decrease in total pore volume for aerogels X26, X39, and X > 100 with V_{tot} = 1.30, 1.09, and 0.26 mL/g, respectively, as the fraction of undetected pores increases; see Table 2.

Scanning electron microscopy, SEM, images are compared in Figure S1 in the Supporting Information, revealing a network of large macropores with diameters, D, exceeding 1000 nm for X > 100, while aerogel X39 appears to be more dense.

Nanoconfinement of $NaAlH_4$ was performed by melt infiltration at elevated hydrogen pressure to suppress decomposition of $NaAlH_4$ (T = 189 °C, $p(H_2)$ = 210–230 bar). The amount of $NaAlH_4$ was adjusted to obtain the same degree of pore filling of approximately 60 vol % in the mesoporous aerogels; see Table 2. The samples of nanoconfined $NaAlH_4$ are denoted X7-Na, X10-Na, etc.

3.2. In Situ X-ray Diffraction Study of $NaAlH_4$ Nanoconfinement. The melt infiltration process of bulk $NaAlH_4$ into aerogels X13 and X > 100 was studied using in situ synchrotron radiation powder X-ray diffraction, SR-PXD, in the temperature range of RT to 189 °C at a hydrogen pressure of $p(H_2)$ = 160–190 bar; see Figures 1A below and S2 in the Supporting Information, respectively. Diffraction from bulk $NaAlH_4$ is visible from RT and up to ~170 °C where melting occurs. $NaAlH_4$ is expected to be stable at these conditions, but partial decomposition and formation of solid aluminum are observed.[8,9] The intimate contact between the aerogel surface and molten $NaAlH_4$ appears to facilitate decomposition in accordance with previous studies.[16,23] The temperature was kept constant at T = 189 °C for 15 min to ensure complete infiltration of molten $NaAlH_4$ into the respective porous scaffolds. Then, the samples were cooled to RT, and diffraction from confined $NaAlH_4$ becomes visible as it crystallizes inside the pores of aerogel X13 and X > 100, respectively; see Figures 1A and S2.

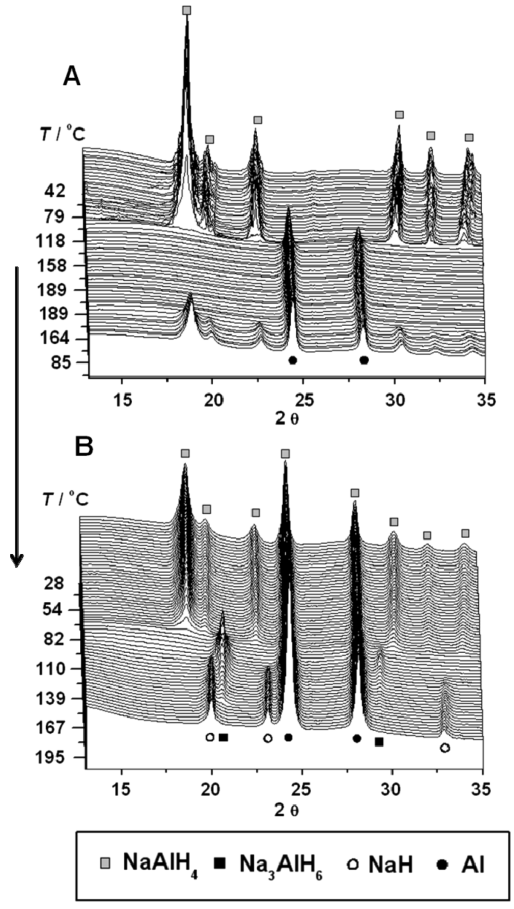

Figure 1. In situ synchrotron radiation powder X-ray diffraction (SR-PXD) data of bulk $NaAlH_4$ mixed with aerogel X13. (A) Samples were heated from RT to 189 °C and kept at fixed temperature for 15 min and then cooled to RT at $p(H_2)$ = 160 bar (heating and cooling rates of 5 and 10 °C/min) to obtain nanoconfined $NaAlH_4$ (sample X13-Na). (B) Dehydrogenation of sample X13-Na (continuation of the experiment in panel A, using the same sample) by heating from RT to 215 °C under dynamic vacuum ($\Delta T/\Delta t$ = 5 °C/min, λ = 0.989 Å). Time propagates from top to bottom.

The full width half-maximum, fwhm, for the Bragg diffraction peaks before and after melt infiltration is extracted from Rietveld refinements of the in situ SR-PXD data in Figure 1A and S2 in the Supporting Information. For sample X13-Na, the

dx.doi.org/10.1021/jp3049982 | J. Phys. Chem. C 2012, 116, 21046–21051

diffraction peaks from melt-infiltrated $NaAlH_4$ are significantly broadened as compared to the bulk $NaAlH_4$ indicating formation of nanocrystallites by nanoconfinement. The average apparent crystallite size of $NaAlH_4$ in sample X13-Na is determined to be ∼30 nm, while no size-related peak broadening is observed for Al indicating that it resides on the external surface of the scaffold; see the Supporting Information. In contrast, fwhm parameters for bulk and melt-infiltrated $NaAlH_4$ for sample X > 100-Na are similar; i.e. larger crystallites are formed in the absence of nanopores (see Figure 2S).

The melt-infiltrated sample X13-Na, prepared in situ (Figure 1A), was further investigated in order to study the dehydrogenation mechanism of nanoconfined $NaAlH_4$; see Figure 1B. The diffracted intensity from $NaAlH_4$ gradually decreases and fully disappears at a temperature of 135 °C with the contemporary formation of Na_3AlH_6. Diffraction from Na_3AlH_6 is visible in the temperature range 136−190 °C, and NaH forms at $T \sim 150$ °C. The observed dehydrogenation mechanism is in accordance with that of bulk $NaAlH_4$; see reaction scheme I. However, recent theoretical calculations predict that the formation of Na_3AlH_6 nanoparticles is unfavorable.[25] In this study, Rietveld refinements were used to investigate fwhm parameters of Na_3AlH_6, NaH, and Al, and no size-induced Bragg peak broadening was observed. This may be due to a pronounced destabilization of Na_3AlH_6 and NaH, which may lead to a fast decomposition to liquid sodium and some agglomeration of the reaction products on the external surface of the aerogel. Therefore, nanoconfined $NaAlH_4$ may migrate out of the porous scaffold during release of hydrogen and crystallize as larger particles on the surface of the scaffold. The investigations show no indications for chemical reactions between the scaffold and $NaAlH_4$.

3.3. Effects of Pore Size on the Hydrogen Desorption Kinetics. The first hydrogen desorption is investigated for all samples using temperature-programmed desorption mass spectroscopy, TPD-MS; see Figure 2. The onset temperature for hydrogen release, T_{onset}, and the temperature for maximum relative H_2 desorption rate, T_{max}, are compared in Table 3.

These results show that melt infiltration of $NaAlH_4$ into aerogel X > 100 improves the kinetics significantly as compared to bulk $NaAlH_4$ ($\Delta T_{max} = -90$ °C and $\Delta T_{onset} \sim -100$ °C), despite the absence of nanopores and formation of metal hydride nanoparticles. These results indicate that the aerogel surface acts as a catalyst for $NaAlH_4$ decomposition. The TPD-MS T_{max} temperatures are plotted as a function of the aerogel pore size in Figure 3A. Presence of nanopores and formation of metal hydride nanoparticles further reduce the hydrogen release temperatures revealed by comparing sample X39-Na and X > 100-Na ($\Delta T_{max} = -12$ °C and $\Delta T_{onset} \sim -25$ °C). Further reduction of the aerogel pore size, D_{max}, from 39 to 19 nm does not influence T_{max}, which is 150 °C. The T_{max} temperatures for samples X19-Na, X13-Na, X10-Na, and X7-Na are 150, 149, 147, and 146 °C, respectively, indicating that smaller pores mediate slightly lower temperatures for maximum hydrogen release rates. However, the beneficial effect of introducing nanopores is small relative to the catalytic effect induced by the aerogel surface. The effect of lowering the pore size from 7 to 4 nm is in fact an increase in the dehydrogenation temperature to $T_{max} = 171$ °C indicating existence of a lower limiting pore size for the infiltration of molten $NaAlH_4$ in the used carbon aerogel scaffolds. Noteworthy, the kinetics are still considerably improved as compared to bulk $NaAlH_4$ ($\Delta T_{max} = -81$ °C) owing to the catalytic properties of the carbon aerogel.

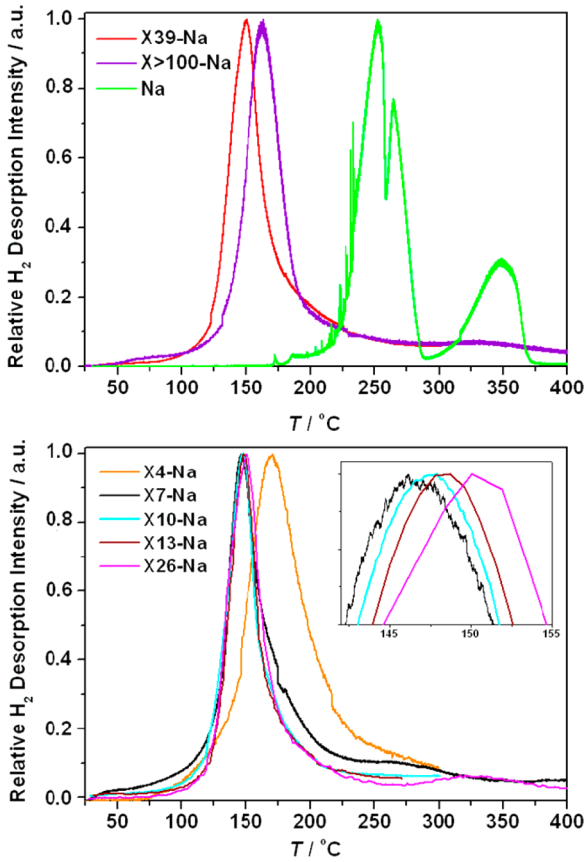

Figure 2. Normalized TPD-MS data collected from RT to 400 °C ($\Delta T/\Delta t = 1$ °C/min) by recording the mass spectrometer intensity of H_2^+ ions ($m/e = 2$). (A, top) Relative hydrogen desorption intensities for samples of bulk $NaAlH_4$ (Na, green), X > 100-Na (purple), and X39-Na (red). (B, bottom) Relative H_2 desorption intensities for samples X4-Na (orange), X7-Na (black), X10-Na (teal), X13-Na (brown), and X26-Na (pink).

Table 3. Temperature for the Onset of Hydrogen Release, T_{onset}, and the Maximum of the Relative Hydrogen Desorption Intensity, T_{max}, for the Major Hydrogen Release Peaks

sample	D_{max}	T_{onset}/°C	T_{max}/°C[b]
X4-Na	4	75	171
X7-Na	7	60	146
X10-Na	10	75	147
X13-Na	13	75	149
X19-Na[a]	19	75	150
X22-Na[a]	22	75	149
X26-Na	26	75	150
X39-Na	39	75	150
X > 100-Na	>100	100	162
Na	–	200	252

[a]The TPD-MS profile is shown in the Supporting Information. [b]The uncertainties for the estimated T_{onset} and T_{max} temperatures are ±5 and 0.5 °C, respectively.

The average crystallite sizes of nanoconfined $NaAlH_4$ were estimated from Rietveld refinements (possible stress and strain was neglected in the calculations) and reveal a linear correlation with the aerogel pore size; see Figure 3B and the Supporting Information. Clearly, the smaller pores facilitate the formation of smaller $NaAlH_4$ nanocrystallites. However, the reduction in

dx.doi.org/10.1021/jp3049982 | J. Phys. Chem. C 2012, 116, 21046−21051

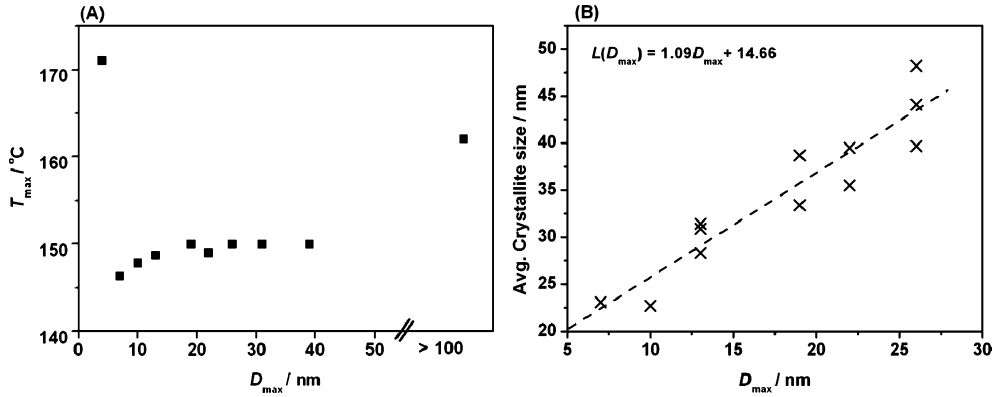

Figure 3. (A) Maximum temperature for hydrogen release, T_{max}, measured by TPD-MS as a function of aerogel pore size, D_{max}. (B) Average crystallite size, L, of nanoconfined $NaAlH_4$ determined using SR-PXD data and plotted as a function of D_{max}. Different fractions of the same sample were measured and analyzed up to three times.

crystallite size only introduces a minor improvement of the hydrogen release kinetics, i.e., reduction of T_{max}; see Figure 3A. Recent experimental and theoretical studies reveal significant decrease in hydrogen release onset temperatures for $NaAlH_4$ only for particles smaller than ~10 nm.[25,26] In this study, the crystallites for nanoconfined $NaAlH_4$ obtained by melt infiltration are too large (>23 nm) for further significant improvements in the hydrogen release kinetics. It is noted that the average crystallite size of melt-infiltrated $NaAlH_4$ is larger than the average pore size of the respective aerogels, D_{max}, derived by gas sorption (Table 2). This may suggest that crystallization preferably takes place in the larger pores in the aerogel.[16]

3.4. Stability and Kinetics. The prolific effects on the hydrogen release and uptake originating from the nanopores and the catalytic carbon surface, respectively, are investigated for samples X13-Na and X > 100-Na using Sieverts' measurements; see Figure 4. Sample X13-Na releases 3.5, 2.4, 2.0, and 1.9 wt % $H_2/NaAlH_4$ during desorptions 1−4, respectively; see Figure 4a. Considering the additional weight provided by the scaffold material, a total of 1.1 wt % H_2 is released from sample X10-Na during the first desorption. The sample releases 67.7, 58.1, and 53.8% of the initial hydrogen content during desorption 2, 3, and 4, respectively. The amount of hydrogen released is lower than 5.6 wt % due to partial decomposition of $NaAlH_4$ during melt infiltration; see Figure 1. Sample X > 100-Na releases 3.9, 2.6, 2.2, and 2.0 wt % $H_2/NaAlH_4$ during desorption 1−4 corresponding to 65.9, 55.8, and 52.1% of the initial hydrogen content during desorption 2, 3, and 4. Thus, nanopores in sample X10-Na and macropores in sample X > 100-Na appear to have a similar ability to preserve the hydrogen storage capacity.

The results presented here indicate that the catalytic carbon surface is mainly responsible for the beneficial properties induced by nanoconfinement of $NaAlH_4$ in carbon aerogel scaffolds, which may not be the case for other metal hydrides. For example, $LiBH_4$ was successfully melt-infiltrated in microporous carbon (D_{max} < 2 nm) as well as carbon aerogels with pore sizes of 13 and 25 nm, respectively.[27] The smaller pores facilitated faster hydrogen release kinetics and improved reversible hydrogen storage capacity.[2,4,27]

4. CONCLUSIONS

$NaAlH_4$ was melt-infiltrated into aerogels with pore sizes of 4, 7, 10, 13, 19, 22, 26, 39, and >100 nm. Nanocrystallites were

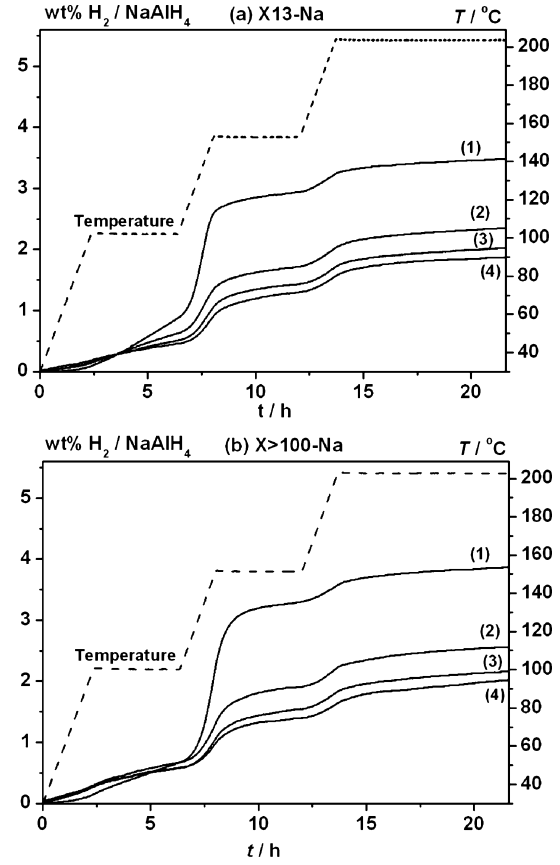

Figure 4. Sieverts' measurements showing hydrogen desorption cycles 1−4 for samples (a) X13-Na and (b) X > 100-Na. Hydrogen desorption was performed at fixed temperatures of 100, 152, and 203 °C ($\Delta T/\Delta t$ = 0.5 °C/min). Hydrogen absorption was performed at 160 °C and $p(H_2)$ ~ 92 bar for 10 h.

only formed in the nanoporous scaffolds with 4 < D_{max} < 100 nm. The temperature for maximum hydrogen release rate measured by TPD-MS, T_{max}, decreased from 252 °C for bulk $NaAlH_4$ to 162 °C by melt infiltration into the macroporous aerogel (>100 nm). This improvement is assigned mainly to the catalytic properties of the carbon aerogel surface possibly with a small contribution from confinement in mesopores. Additional improvement is induced by reducing the pore sizes in the range 7 ≤ D_{max} ≤ 39 nm and thereby the $NaAlH_4$

dx.doi.org/10.1021/jp3049982 | J. Phys. Chem. C 2012, 116, 21046−21051

crystallite sizes, but this effect is small (ΔT_{max} = −12 to −16 °C) relative to the catalytic effects induced by the aerogel surface. The crystalline domain size observed using PXD is larger than the pore size and linearly correlated. This work suggests that a significant contribution to the observed improvements of kinetics by nanoconfinement of $NaAlH_4$ in carbon aerogels can be assigned to the catalytic properties of the scaffold surface and a minor contribution arises from size effects introduced by nanoconfinement in scaffolds with pore sizes in the range of 39−7 nm.

■ ASSOCIATED CONTENT

Supporting Information

Homogeneity study of aerogel X10, crystallite size calculations using Rietveld refinements, and TPD-MS profiles for samples X19-Na and X22-Na. This material is available free of charge via the Internet at http://pubs.acs.org.

■ AUTHOR INFORMATION

Corresponding Author

*Email: trj@chem.au.dk.

Notes

The authors declare no competing financial interest.

■ ACKNOWLEDGMENTS

The work was supported by the CarlsbergFondet, the Danish National Research Foundation (Centre for Materials Crystallography), the Danish Strategic Research Council (Centre for Energy Materials), and the Danish Council for Independent Research Natural Science (FNU). The access to beam time at the MAX-II synchrotron, Lund, Sweden in the research laboratory MAX-lab is gratefully acknowledged. We also acknowledge funding from the European Community's Seventh Framework Programme FCH-JU, project Bor4store (303428). We are grateful to the Polish Ministry of Science and Higher Education (Key Project POIG.01.03.01-14-016/08 and POIG.02.01.00-14-071/08/00).

■ REFERENCES

(1) Schlapbach, L.; Züttel, A. *Nature* **2001**, *414*, 353−358.
(2) Nielsen, T. K.; Jensen, T. R.; Besenbacher, F. *Nanoscale* **2011**, *3*, 2086−2098.
(3) Vajo, J. J. *Curr. Opin. Solid State Mater. Sci.* **2011**, *15*, 52−61.
(4) de Jongh, P. E.; Adelhelm, P. *ChemSusChem* **2010**, *3*, 1332−1348.
(5) Gutowska, A.; Li, L. Y.; Shin, Y. S.; Wang, C. M. M.; Li, X. H. S.; Linehan, J. C.; Smith, R. S.; Kay, B. D.; Schmid, B.; Shaw, W.; et al. *Angew. Chem., Int. Ed.* **2005**, *44*, 3578−3582.
(6) U.S. Department of Energy Doe Targets for Onboard Hydrogen Storage Systems for Light-Duty Vehicles. https://www.Eecbg.Energy.Gov/Hydrogenandfuelcells/Storage/Pdfs/Targets_Onboard_Hydro_Storage_Explanation.Pdf.
(7) Rude, L. H.; Nielsen, T. K.; Ravnsbaek, D. B.; Bösenberg, U.; Ley, M. B.; Richter, B.; Arnbjerg, L. M.; Dornheim, M.; Filinchuk, Y.; Besenbacher, F.; et al. *Phys. Status Solidi A* **2011**, *208*, 1754−1773.
(8) Bogdanovic, B.; Brand, R. A.; Marjanovic, A.; Schwickardi, M.; Tölle, J. *J. Alloys Compd.* **2000**, *302*, 36−58.
(9) Gao, J.; Adelhelm, P.; Verkuijlen, M. H. W.; Rongeat, C.; Herrich, M.; van Bentum, P. J. M.; Gutfleisch, O.; Kentgens, A. P. M.; de Jong, K. P.; de Jongh, P. E. *J. Phys. Chem. C* **2010**, *114*, 4675−4682.
(10) Ranong, C. N.; Hohne, M.; Franzen, J.; Hapke, J.; Fieg, G.; Dornheim, M.; Eigen, N.; von Colbe, J. M. B.; Metz, O. *Chem. Eng. Technol.* **2009**, *32*, 1154−1163.
(11) Rongeat, C.; Jansa, I. L.; Oswald, S.; Schultz, L.; Gutfleisch, O. *Acta Mater.* **2009**, *57*, 5563−5570.
(12) Sandrock, G.; Gross, K.; Thomas, G. *J. Alloys Compd.* **2002**, *339*, 299−308.
(13) Bogdanovic, B.; Schwickardi, M. *Appl. Phys. A: Mater. Sci. Process.* **2001**, *72*, 221−223.
(14) Sartori, S.; Knudsen, K. D.; Hauback, B. C. *J. Phys. Chem. C* **2012**, *116*, 3875−3881.
(15) Stephens, R. D.; Gross, A. F.; Van Atta, S. L.; Vajo, J. J.; Pinkerton, F. E. *Nanotechnology* **2009**, *20*, 204018.
(16) Nielsen, T. K.; Polanski, M.; Zasada, D.; Javadian, P.; Besenbacher, F.; Bystrzycki, J.; Skibsted, J.; Jensen, T. R. *ACS Nano* **2011**, *5*, 4056−4064.
(17) Lohstroh, W.; Roth, A.; Hahn, H.; Fichtner, M. *Chemphyschem* **2010**, *11*, 789−792.
(18) Sartori, S.; Knudsen, K. D.; Roth, A.; Fichtner, M.; Hauback, B. C. *Nanosci. Nanotech. Lett.* **2012**, *4*, 173−177.
(19) Berseth, P. A.; Harter, A. G.; Zidan, R.; Blomqvist, A.; Araújo, C. M.; Scheicher, R. H.; Ahuja, R.; Jena, P. *Nano Lett.* **2009**, *9*, 1501−1505.
(20) Pinkerton, F. E. *J. Alloys Compd.* **2011**, *509*, 8958−8964.
(21) Nielsen, T. K.; Manickam, K.; Hirscher, M.; Besenbacher, F.; Jensen, T. R. *ACS Nano* **2009**, *3*, 3521−3528.
(22) Al-Muhtaseb, S. A.; Ritter, J. A. *Adv. Mater.* **2003**, *15*, 101−114.
(23) Adelhelm, P.; Gao, J. B.; Verkuijlen, M. H. W.; Rongeat, C.; Herrich, M.; van Bentum, P. J. M.; Gutfleisch, O.; Kentgens, A. P. M.; de Jong, K. P.; de Jongh, P. E. *Chem. Mater.* **2010**, *22*, 2233−2238.
(24) Jensen, T. R.; Nielsen, T. K.; Filinchuk, Y.; Jorgensen, J.-E.; Cerenius, Y.; Gray, E. M.; Webb, C. J. *J. Appl. Crystallogr.* **2010**, *43*, 1456−1463.
(25) Mueller, T.; Ceder, G. *ACS Nano* **2010**, *4*, 5647−5656.
(26) Balde, C. P.; Hereijgers, B. P. C.; Bitter, J. H.; de Jong, K. P. *J. Am. Chem. Soc.* **2008**, *130*, 6761−6765.
(27) Gross, A. F.; Vajo, J. J.; Van Atta, S. L.; Olson, G. L. *J. Phys. Chem. C* **2008**, *112*, 5651−5657.